Article

Ultralow-frequency seismic sounding of railway subgrade state by passing trains

Galina N. Antonovskaya [ID][a], **Irina P. Orlova** [ID][b], and **Natalia K. Kapustian**[a,b]

[a]N. Laverov Federal Center for Integrated Arctic Research of the Ural Branch of the Russian Academy of Sciences, Arkhangelsk, Russia; [b]Schmidt Institute of Physics of the Earth of the Russian Academy of Sciences, Moscow, Russia

Corresponding author: **Galina N. Antonovskaya** (email: essm.ras@gmail.com)

Abstract

The degradation of the railway subgrade is a common cause for train accidents in Russia because of the extensive railway system and large areas of weak soils. We present a seismic monitoring technique that utilizes moving trains as signal sources to probe the properties of the subgrade. The broadband (periods up to 100 s) seismic sensors recorded signals over several weeks during a nonstop monitoring experiment. The large statistic allows us to identify the signals properties, and thus these signals are processed by an automated system. We defined the parameters of the low-frequency signal generated by a passing train that are sensitive to changes in the subgrade state. These are the ratio of amplitudes of horizontal components, and the time interval between the end of the train passage and the maximum amplitude surge in the component transversal to rails. We propose an analytical model to describe the interaction between a moving train and the subgrade that takes into consideration the viscosity of a substrate layer. The application of this model produces a consistent explanation of processes in the media and enables an "in situ" estimation of soil elasticity and viscosity, caused by seasonal thawing.

Key words: railway subgrade stability, low-frequency vibrations, seismic test, seismic equipment, simulation

Résumé

La dégradation de la sous-fondation des voies ferrées est une cause fréquente d'accidents ferroviaires en Russie, en raison de l'étendue du réseau ferroviaire et des grandes zones de sols fragiles. Nous présentons une technique de surveillance sismique qui utilise des trains en mouvement comme sources de signaux pour sonder les propriétés de la plate-forme. Les capteurs sismiques à large bande (périodes jusqu'à 100 s) ont enregistré des signaux pendant plusieurs semaines au cours d'une expérience de surveillance ininterrompue. La grande statistique nous permet d'identifier les propriétés des signaux et ainsi ces signaux sont traités par un système automatisé. Nous avons défini les paramètres du signal basse fréquence généré par le passage d'un train qui sont sensibles aux changements de l'état de la plate-forme. Il s'agit du rapport des amplitudes des composantes horizontales, et de l'intervalle de temps entre la fin du passage du train et la poussée maximale d'amplitude de la composante transversale aux rails. Nous proposons un modèle analytique pour décrire l'interaction entre un train en mouvement et la plate-forme qui prend en compte la viscosité d'une couche de substrat. L'application de ce modèle produit une explication cohérente des processus dans le milieu et permet une estimation « in situ » de l'élasticité et de la viscosité du sol, causées par le dégel saisonnier. [Traduit par la Rédaction]

Mots-clés : plate-forme ferroviaire stabilité, vibrations basse fréquence, test sismique, équipement sismique, simulation

Introduction

More than 65% of Russian territory is cryolithozone where soils remain frozen for many consecutive years (permafrost) (Garagulia and Ershov 2000; Fig. 1) and more than 15 million residents of Russia live in these territories. Latter regions often contain watered and swampy weak soils especially in the northern part of European Russia. These conditions complicate railroad construction works and require special measures to ensure the safety of operation, namely, soil characterization and reinforcement. These include enforced antithawing and the construction of reinforced substrate layers on top of frozen soils (Ashpiz et al. 2011; Kudryavtsev et al. 2016; Kondratiev 2017; Zhang et al. 2018).

The railroad safety is threatened by landslides, mudslides, melting of permafrost, carst, subsidence, rockfall, snow slides, etc. Deformation of the subgrade soils happens across 4%–10% of railways with inhomogeneous distribution: 1%–3% in the European part with better soils and 15%–25% in extreme regions of the Eastern Siberia and Far East. Additionally, the planned increase in the trains' speed and the carrying capacity of vehicle till 27 t axle load (Russian Railways Company Standard 10.002–2015 2016; Railvolution 2019) are

Fig. 1. Permafrost distribution in the Russian Federation (Kotlyakov and Khromova 2012). Zones represent the permafrost density and thickness. Permafrost depth in region 2 is above 50 m, in region 3 it is 50–90 m, and in region 4 it is below 90 m. [Colour online]

factors of existing and new dangerous phenomena. The soil monitoring methods and techniques that are aimed to prevent the formation of defects or to fix the existing ones are still the same (Ma et al. 2012; Varlamov 2018; Tian et al. 2021).

There is a plethora of methods used worldwide to ensure the safety of railroad operation by probing the railway subgrade state: traditional (visual, geodesic, hydrogeological, and thermometric), geophysical (electrometric, radio location, and seismic), or mobile complexes including aerospace (Szwilski et al. 2003, 2004; Ižvolt et al. 2016; Kovacevic et al. 2016; Fraga-Lamas et al. 2017; NetworkRail 2018; Brzeziński et al. 2018). We will focus on the following seismic methods: traditional shallow seismic survey profiling and the registration of vibrations produced by passing trains (Aw 2007; Donohue et al. 2011; Ashpiz et al. 2011 ; Sukhobok et al. 2016; Mirzaxidova 2020).

There are three common points for most of the seismic methods used. First, the frequency of the probing signal is above 5 Hz. Initial studies of the subgrade were performed using the seismic prospection sensors as these are most fitting for building the cross-sections of the railroad embankment. Later the same sensors are used for vibration measurements in the transport constructions. Single-component seismic prospection sensors are well fitted to these tasks also because only the vertical component is usually of interest.

Second common feature is the specification of propagation velocities of longitudinal and transverse waves and the analysis of the train-generated signal dumping (Ashpiz et al. 2011). Finally, all the surveys are discrete in time because the installation procedure for a multiprofile survey system is elaborate and time consuming. The additional factor is that all hazardous processes as the degradation of permafrost and watering are very slow.

Seismic profile reconstruction requires wave arrival times and is limited to the depth of 3–4 m (Szwilski et al. 2003, 2004). An example of the resulting structure cross-sections with wave velocities and the relief of layers is given in Antonovskaya et al. (2020*a*). The accuracy of wave velocities' estimation is comparable with their variations caused by moisture saturation of the ground (Bachrach and Nur 1998; Crane 2013). This in turn makes an early detection of the natural flooding impossible.

The detection of the soil alteration is limited to the surface soil layer because of the amplitude dampening data being collected only for few meter long distances. Only specific seismic and georadar surveys (Szwilski et al. 2003; Fontul et al. 2018) reach deeper layers, which are actually housing the hazardous processes of the soil degradation. Therefore, common methods defined by normative standards (Lehtonen 2011; McHenry and Rose 2012; Authority Transport Asset Standards 2021) can effectively detect the failure in the railroad bank only when it is developed into a hazardous state or even visually pronounced. Seismic probing studies of geologic media show that wave amplitudes are more sensitive to medium deformation by the flooding due to HPP reservoir fill-up or even earthquake development (Gupta and Rustogi 1976; Mashinskii 2005; Zaima and Katayama 2018). This implies that the amplitude-based method can detect soil condition changes at the early stages. The main difficulty in the way of such a method is the reproducibility of a probing signal. To overcome this issue, usually a special signal source is employed: a vibrator (Weber and Münch 2014; Kovalevsky et al. 2020) or an artificial monochrome signal (Kapustian and Yudakhin 2007).

However, there is another way, which is a statistical analysis of amplitudes at frequent impacts. This opportunity has not been exploited before because of the lack of proper signal

Fig. 2. The installation diagram of a seismic station for the railway subgrade monitoring: (*a*) map of the research area where the work place is marked with an asterisk; (*b*) view after installation; (*c*) equipment installation diagram: 1, berm; 2, TC-120s sensor installed in the subgrade; 3, datalogger; 4, storage battery; 5, solar panel; 6, railway track. [Colour online]
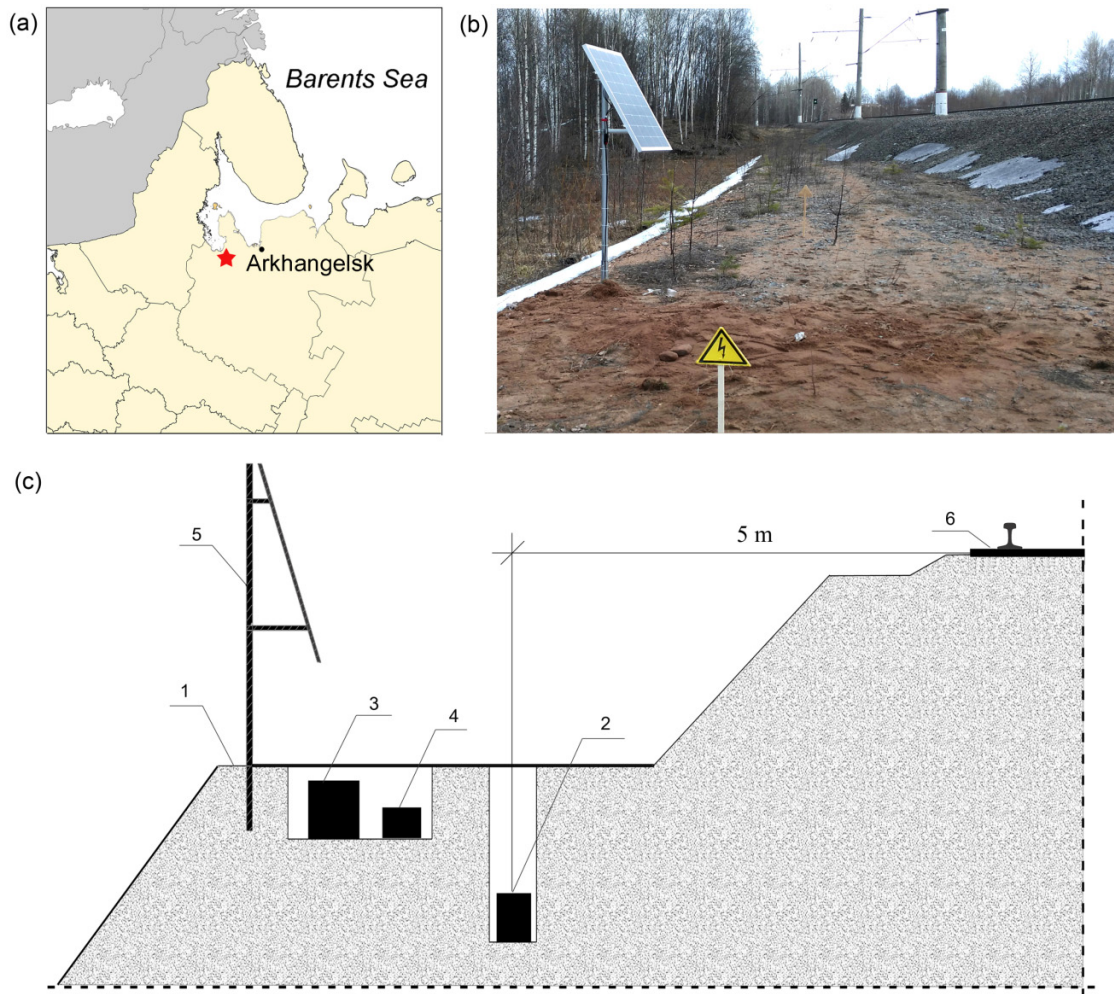
generators. In our study, we assume passing trains as such source and their amount varies from tens to hundreds per day. The resulting impact contains at least three types of vibration and dynamic loads with different parameters. First of all, mechanical oscillations from train wheels passing over rail gaps propagate over hundreds of meters away from a railway (Basakina et al. 2014; Connolly et al. 2014*a*, 2014*b*). The characteristic frequencies of such waves are above 5 Hz, and these vibrations are useful for the estimation of vibrational impacts on buildings (Lopes et al. 2016; Hu et al. 2018).
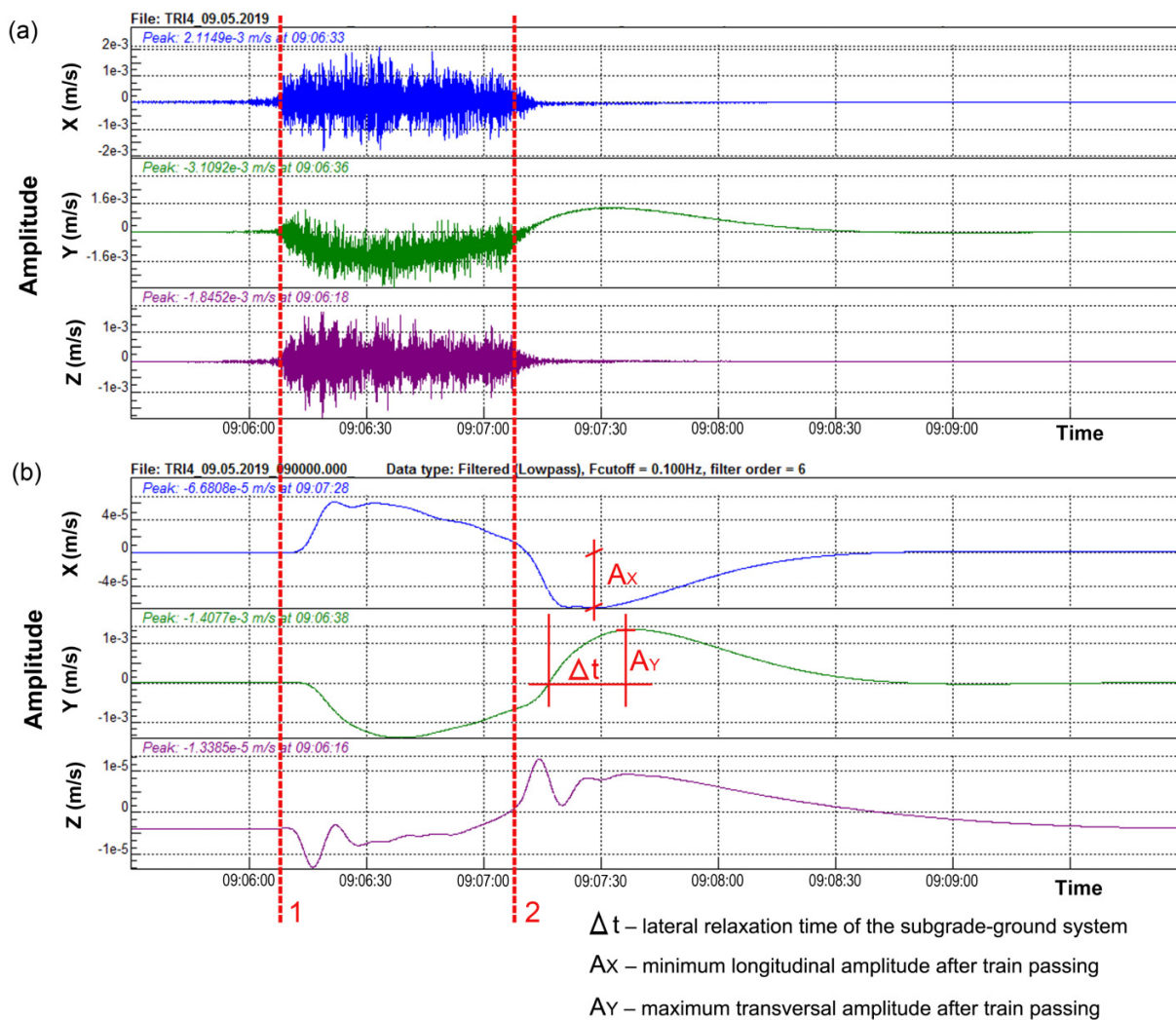
Another interaction is a wheel deforming a rail subgrade. The impact propagates to sleepers and the upper layer of the subgrade (Grassie et al. 1982; Brough et al. 2003; Antonovskaya et al. 2021). The subgrade deformation study is performed with a variety of sensors (load cells, borehole deformation gauges techniques, etc.) (Hendry et al. 2008; Ngamkhanong et al. 2018) using nondestructive testing methods, namely, seismic surface-wave and ground-penetrating radar survey (Anbazhagan et al. 2011). The resulting loads and deformations are large enough to treat the

passing train as a source similar to ones used for dynamic soil probing (Pinzon-Rincon et al. 2021).

While these types of vibromechanical impacts are studied (Krylov 1997; Picoux and LeHouédec 2005; Stoyanovich and Pupatenko 2015; Burdzik and Nowak 2017), they are not used for early fault detection in soil. Particularly, Mirzaxidova (2020) in her study points out that the problem of a timely detection of hazardous regions in the railroad subgrade cannot be resolved in the current decade.

Finally, the moving train not only compresses the track foundation, i.e., vertical forces act, but also can push it in a horizontal plane. The latter is possible if subsoil or natural ground is the elasto-viscous medium (i.e., low-velocity layer) compared to the track foundation. The track foundation is restored after removing the load (passing the train) and the deformation–recovery curve has a hysteresis loop, and we have observed this in our studies (Antonovskaya et al. 2020*b*). The mentioned article is a pioneering study made possible by never used before ultralow-frequency sensors with three-component registration for railroad subgrade monitoring.

Fig. 3. Characteristic seismic waveforms produced by a cargo train: (*a*) original waveforms; (*b*) waveforms after 0.1 Hz low-pass filtering. Vertical lines are timestamps for (1) train head and (2) train tail passage. [Colour online]

Δt – lateral relaxation time of the subgrade-ground system

A_X – minimum longitudinal amplitude after train passing

A_Y – maximum transversal amplitude after train passing

As we inspect low-frequency oscillations in both horizontal and vertical axes for parameters that can be used in monitoring, we have to keep in mind that those parameters are to be least dependent on a source type (train's weight, speed, etc.) and are easy to process for an automated system connecting a multitude of remote sensors. We also focus on the reaction of these parameters to the climate-related changes, such as spring temperature oscillations and thawing of soils, to estimate how sensitive the method is toward the shifts in subgrade soil state.

Main goal of our study is the search for seismic waveform parameters that are informative for detecting changes in the subgrade and are available for automated record processing.

Materials and methods

The experiment took place in the Onega district of Arkhangelsk region, north of the Russian Federation, on the Northern Railway of JSC "Russian Railways" (Fig. 2*a*). The chosen railway section lies in peaty soils. Embankment's height

is 3 m. We used three-component broadband seismic sensors TC-120s from Nanometrics (Kanata, ON, Canada). The installation of the seismic station and its location are shown in Fig. 2. Sensors were buried 80 cm deep and 5 m away from the railway. The X component is aligned with the railway, Y is horizontally perpendicular, and Z is vertical. We placed the datalogger (3) and the storage battery (4) in a separate metal box which we also buried next to the seismic sensor. As a result, a solar panel for powering the system and a GPS antenna remained on the Earth's surface. Special signs marked the locations of the equipment (Fig. 2*b*). The equipment operated in continuous mode; data were recorded on the datalogger flash storage. The observations conducted between 23 April and 17 July 2019 captured 1590 various trains during this period, including single locomotives, passenger trains, and empty and loaded cargo trains.

A typical set of waveforms registered when cargo trains pass by the monitoring point is shown in (Fig. 3*a*). The average weight of a cargo train is 4000 tons, the speed is 45–55 km/h, and about 30–40 trains pass along the track per day, which characterizes a constant technogenic load on the

Fig. 4. Low-frequency oscillation parameters for eight cargo trains: (*a*) waveforms for Y component for period "train passing–lateral relaxation time". Curves are drawn one under the other, the ends of trains' passage are marked by vertical dotted line. (*b*) Trajectories of ground particles motion in the horizontal plane for the same period.
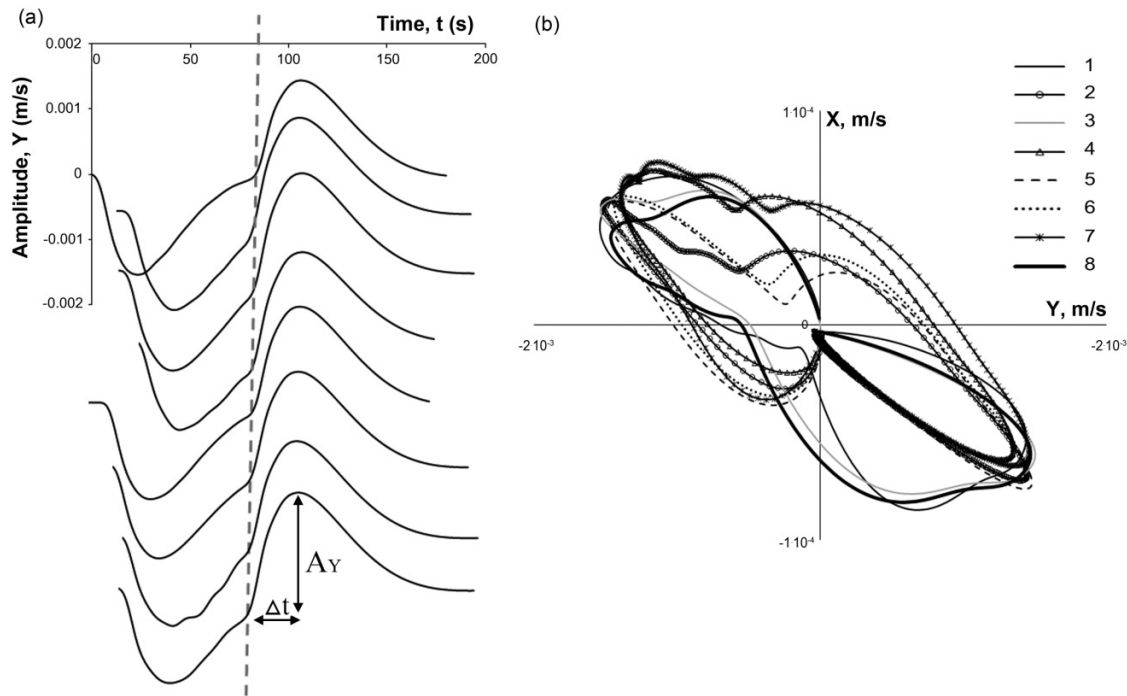
weak soils. Transversal horizontal oscillations (Y) are dominating but there are two distinctive set of frequencies. To process the most impactful low-frequency part of the signal, we do noise reduction by short-time-average through long-time-average (STA/LTA) trigger algorithm, which is common in seismology for an automatic event detection (Trnkoczy 2012). The next step is low-pass filtering of frequencies below 0.1 Hz (Fig. 3*b*). To identify the stable, i.e., recurring, waveform properties, we looked through the filtered recordings. For the Z component, the recurring feature is periods of a sinusoid at the beginning of the recording and at the end of the train passage—vertical lines mark the passing interval. It is only visible on the filtered waveforms and its presence is derived analytically when solving the task of deformation of the roadbed by a passing train (Antonovskaya et al. 2021). The amplitude and period of the first sinusoid are the most informative and reproducible and are sensitive to a sensor position, head locomotive weight and speed, and elastic soil parameters.

Another tool in our arsenal is time-series plotting of the chosen parameters alongside with temporal variations of external factors like temperature.

Experimental results

Low-frequency oscillations last much longer than high-frequency oscillations and persist beyond the train passage time (Fig. 3). We observe that the waveform of the passing train heavily depends on train velocity and acceleration/deceleration and its weight and length but waveforms

subgrade oscillations after passing trains are similar (Fig. 4). Additionally, the amplitude maximum A_Y for component Y is one–two orders of magnitude higher than A_X for component X in the relaxation part (Fig. 3*b*). Thus, we will consider further only the post-train waveform. Values of maximum (A_Y) and minimum (A_X) amplitudes after the passage of the train and Δt—the interval between zero and maximum A_Y—are shown in Fig. 3*b*.

We registered cargo and passenger trains and single locomotives. Also, different train types on seismic records are clearly separated by the time duration and by the oscillation amplitude values. The average weight varies from 200 tons (single locomotive) to 4000 tons (cargo train). The histogram of A_Y values (Fig. 5) exhibits three local maxima—$A_{Y1} = 0.05 \times 10^{-3}$, $A_{Y2} = 0.4 \times 10^{-3}$, and $A_{Y3} = 1.4 \times 10^{-3}$ m/s—with the last being the strongest. The first maximum corresponds to single locomotives, the second one to passenger trains, and the third one to cargo trains. Single locomotives represent a small group, so we did not consider them separately.

If A_Y is dependent on the train weight, then amplitudes for X and Y components should be proportional. It is clear from the A_X–A_Y diagram (Fig. 6) that there is a dependence. For all data points a linear dependence is clear, and two others that represent heavy and light trains (groups 2 and 3) seem to have parallel linear fits. Remark that approximation reliability for the whole data set (all trains) is better than for groups 2 and 3 due to the larger data amount for the whole data. We show all data within $\pm 3\sigma$ band for maxima 2 and 3. Further, we used data in σ band to obtain better reliability and regarded only cargo trains. The latter suggest that the mass of a train

Fig. 5. Histograms of the different parameters: (*a*) amplitude maximum A_Y for component Y; (*b*) Δt according to the results of processing for the entire period of observations.
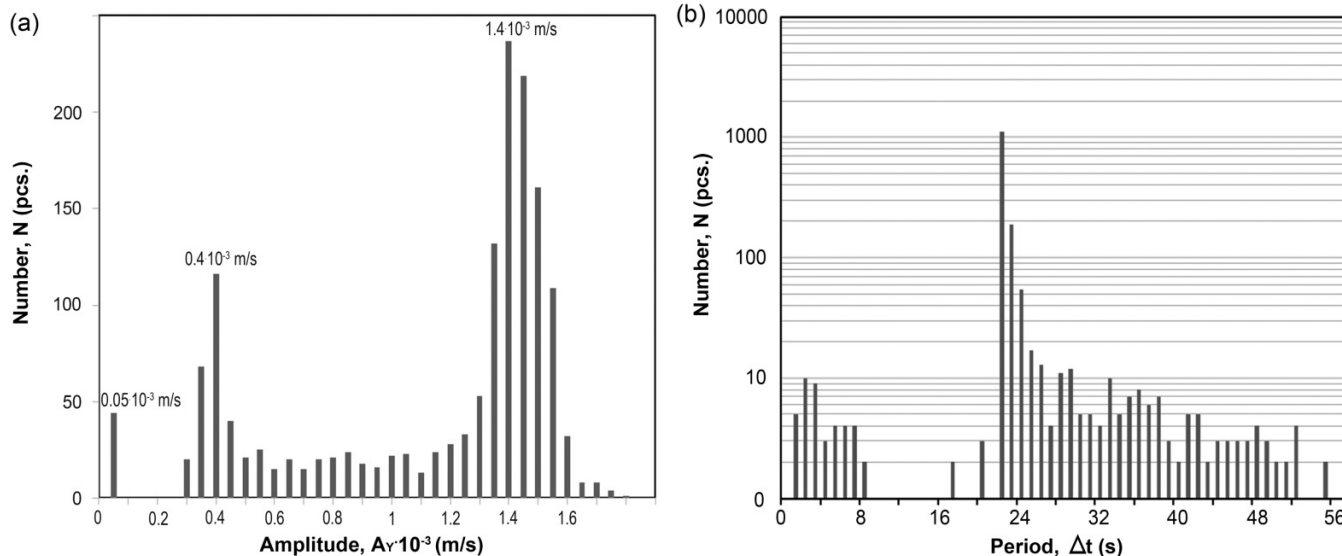
Fig. 6. Scatter chart of horizontal amplitudes A_X–A_Y with linear trend lines for (1) all data and for data groups corresponding to maxima: (2) $A_Y = 0.4 \times 10^{-3}$ m/s; (3) $A_Y = 1.4 \times 10^{-3}$ m/s. Equations and values of the approximation reliability R^2 are shown in Fig. 6. [Colour online]
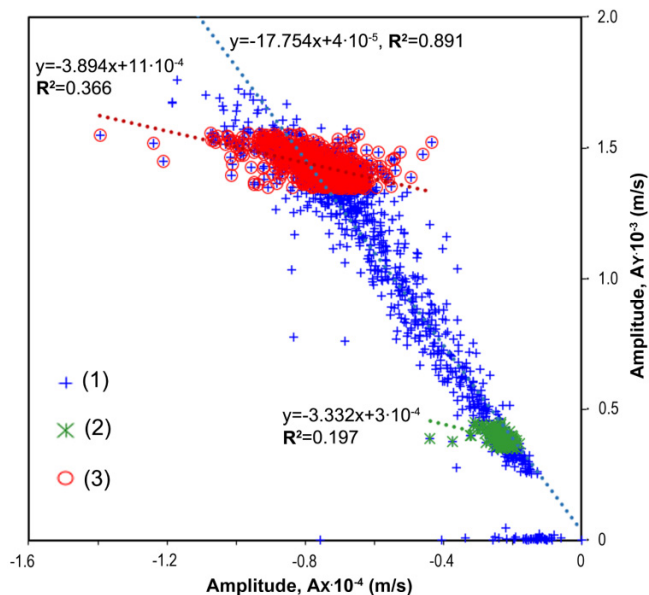
might determine the amplitudes. The linear slope coefficient R is determined as

$$R = \left| \frac{A_Y}{A_X} \right|$$

and is considered to be weight-independent.

Another parameter to be analysed is time interval Δt obtained by the automatic processing. Most of the obtained

values (more than 90%) lie within 20–27 s interval (see the histogram in Fig. 5*b*); therefore, we used only the recordings that have Δt within this range.

Analytical model

The process of low-frequency deformation of the homogeneous soil layer by a passing train can be solved analytically. This is essentially the Boussinesq solution, which we have already successfully employed, and it produces values and waveforms close to experimental ones for the vertical low-frequency (0.5–2 Hz) component (Antonovskaya et al. 2021). The initial low-frequency waveform is almost nondistinguishable for the horizontal component (Fig. 3). However, the horizontal oscillations are well described by the Elsasser model, which examines the elastic layer over a viscous half-space and describes the space–temporal distribution of medium stress. The analytical Boussinesq solution produces the vibration amplitude values, i.e., the parameter obtained by a velocimeter. The Elsasser model describes the change of the stress–strain state that can be used to derive the vibration amplitude (Irvine 2013). Therefore, we can estimate the state of the soil by analysing changes of the low-frequency amplitude over time.

In Mukhamediev et al. (2008), the model is proposed to describe the propagation of stress according to diffusion laws in a horizontal direction from the mid-ocean ridge; the lithosphere consists of an elastic crust and viscous asthenosphere. The model made it possible to explain the delay in platform seismicity relative to the push created by the ridge as well as to estimate the viscosity of the lithosphere. We used the solution obtained in Mukhamediev et al. (2008), but at a different scale level where the initiating push is created by the train, so the viscous medium can correspond to the low-velocity zone, and the upper elastic layer is the overlying soil (Fig. 7).

Fig. 7. The model of stress disturbances transfer created by the train in the subgrade in horizontal direction: (*a*) schematic section of the railway; (*b*) geometry of the subgrade-ground system and perturbation of its stress–strain. [Colour online]
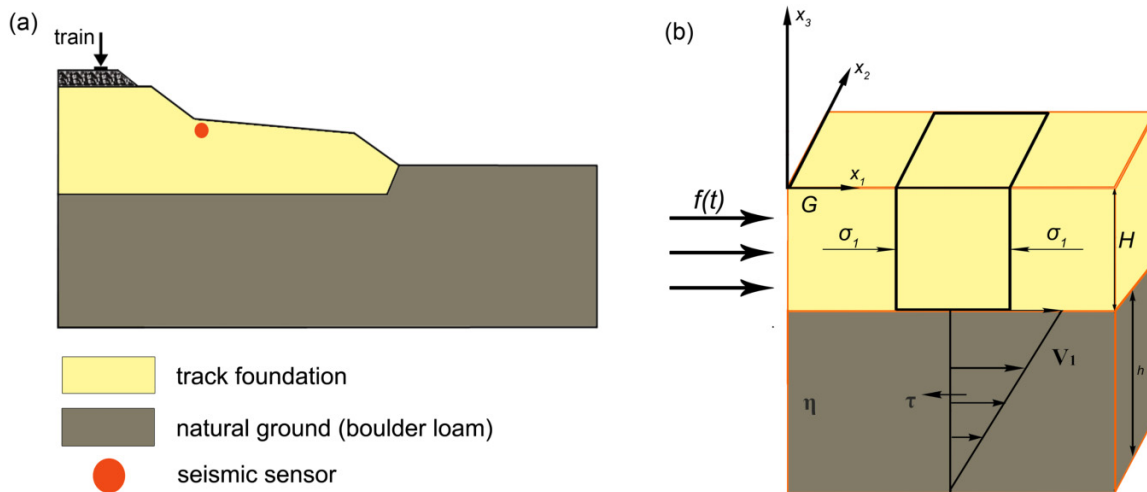
In Mukhamediev et al. (2008), the response to the push was estimated by the change in time of seismicity, so we used the change in time of the amplitude of oscillations at the observation point (broadband seismic equipment location) as a parameter indicating the "arrival" of the impact. This is possible because the amplitude of the vibration velocity is proportional to the additional deformation (Shalev et al. 2015) and thus, for an elastic medium, to the additional stress.

A model of the local tension transmission consists of a rigid elastic embankment (track foundation), underlined by a layer of elastic-viscous soil (natural ground, Fig. 7*b*). The elastic-viscous media may correspond to the low-velocity zone typical of the top part of the cross-section. Tensions propagate along the embankment–soil contact in the horizontal *Y* direction from rails according to diffusion laws (Elsasser 1971). We assume the pressure from the train $p_r =$ const, and it serves as a source of impacts created in the embankment. The process lasts for a time interval *T*, while the disturbances acquire a velocity $V_1(t) > 0$ and an additional stress $\sigma_1(t) > 0$. As a result, it is necessary to determine the propagation function of the disturbance along the *X*-axis $f(x_1, t)$, which satisfies the equation

$$(1) \qquad \frac{\partial f(x_1, t)}{\partial t} = a \frac{\partial^2 f(x_1, t)}{\partial x_1^2}$$

the initial conditions of $f(x_1, 0) = 0$ and $0 < x_1 < \infty$, and the boundary condition:

$$f(0, t) = \begin{cases} 1, 0 < t < T \\ 0, T < t < \infty \end{cases}$$

The coefficient *a* is

$$a = \frac{2G}{\eta(1 - \nu)} Hh$$

where *G* is the shear modulus, η is the viscosity coefficient, ν is the Poisson's ratio, *H* is the embankment thickness, and *h* is the soil thickness.

The analytical solution of (1) is taken from (Carslaw and Jaeger 1989)

$$(2) \qquad f(x_1, t) = \begin{cases} \phi^* \left(\frac{x_1}{2\sqrt{at}} \right), 0 < t < T \\ \phi^* \left(\frac{x_1}{2\sqrt{at}} \right) - \phi^* \left(\frac{x_1}{2\sqrt{a(t-T)}} \right), T < t < \infty \end{cases}$$

where

$$\phi^*(\xi) = 1 - \phi(\xi)$$

and the integral of errors is

$$\phi(\xi) = \frac{2}{\sqrt{\pi}} \int_0^\xi e^{-\xi^2} d\xi$$

where ξ is the integration variable.

The solution of (2) depends on the coefficient *a* and the duration of an impact *T*. For the former one, we took $H = 2.5$ m and $h = 4.5$ m according to the soil slab size and the shallow seismic survey data (Antonovskaya 2020*a*). For the latter, we took an average train passage time of $T = 80$ s. Shear modulus *G* is proportional to the square of the transversal wave velocity V_S and the embankment density ρ:

$$G = V_S^2 \cdot \rho$$

Based on our results of the shallow seismic survey, i.e., $\rho = 1.99$ g/cm^3 and $V_S = 150$ m/s, we obtain $G = 44.8$ MPa. Poisson's ratio is defined by the well-known formula

$$\nu = \frac{V_P^2 \rho - 2G}{2(V_P^2 \rho - G)}$$

Fig. 8. Relative amplitude *A* as a function of time calculated using the Elsasser model for: (*a*) various distances between the sensor and the rails; (*b*) different models and 5 m distance to the rails.
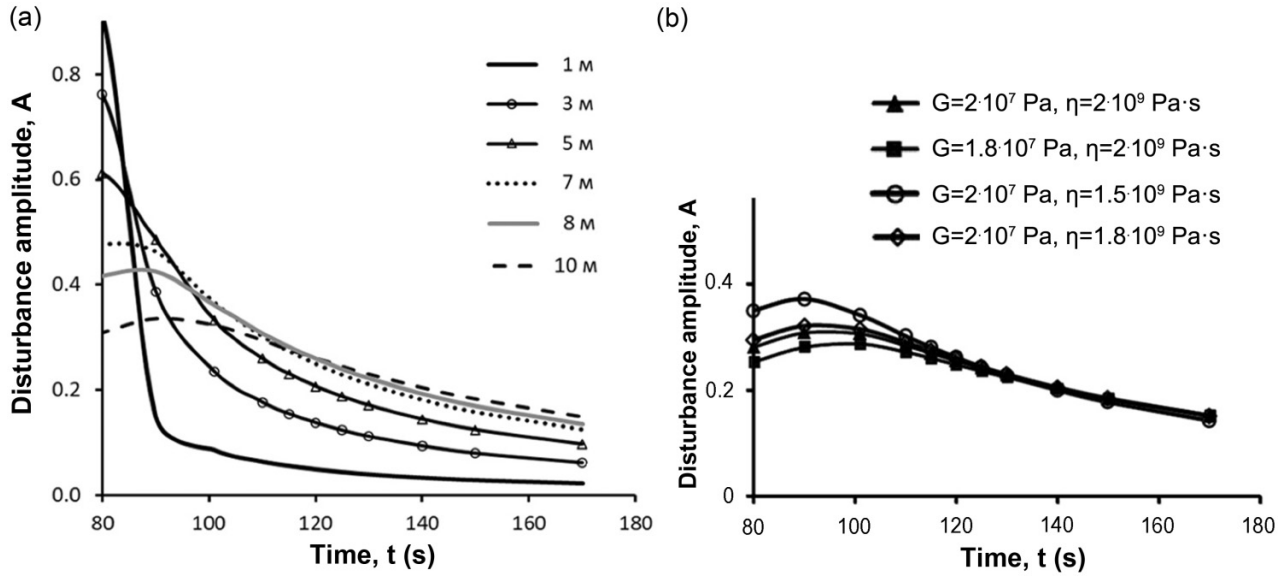
Fig. 9. Evolution of *R*, Δt, N_Y, and the air temperature *T* during the experimental session: (i)–(iii) see in the text. [Colour online]
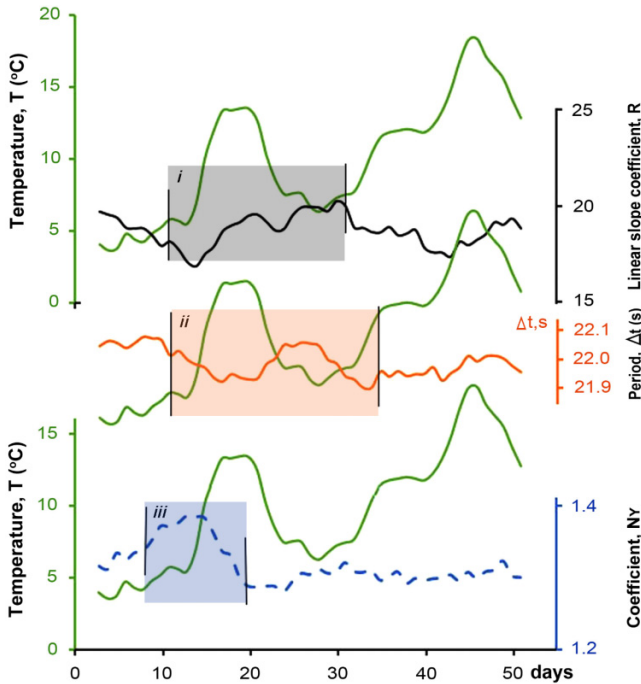
According to the previously mentioned shallow seismic survey data, the average velocities of longitudinal waves V_p for crushed stone-sand embankment vary from 333 to 443 m/s, and thus $v = 0.4$.

Discussion

We calculated the relative perturbation amplitude *A* for different distances from the rails as a function of time past train passage 80 s mark (Fig. 8*a*). The impact maximum decays with the distance and moves later in time—at 5 m it happens at $\Delta t \sim 21$ s. The values and positions of maxima depend on the shear modulus of the upper layer and the viscosity of the lower (Fig. 8*b*). A 10% reduction of *G* leads to an increase of Δt by 5 s and a slight decrease of amplitudes. If viscosity η is reduced by the same 10% interval, then Δt shifts by −1 s and amplitudes stay almost the same. Higher reduction of η further moves Δt to the left and amplitudes rise. In a real case of flooding, *G* will grow and η will decrease; thus, Δt should decrease if the amplitude rises.

We used automated processing on the recordings between April and June 2019 in accordance with the previously explained corrections to retrieve *R* and Δt values. It is reasonable to average these values since there are 30–40 trains passing each day. Given that early stages of hazardous processes in soils can take days and that cargo cycles are week long, we averaged *R*, *Ry*, Δt, and *T*; the chosen method is 7-point moving average (Fig. 9). One has to keep in mind that curve edges, i.e., the first and last weeks, are subjects to larger errors.

The most representative condition (weather, season) parameter is temperature, and it is plotted with 7-day averaging in all instances of Fig. 9. Parameter *R* characterizes mostly a change of the amplitude in the transverse direction, as the soil and embankment are homogeneous in the longitudinal direction. Parameter N_Y is defined as the ratio of median values of the power of vibrations on the Y and Z components; it is a parameter related to high-frequency oscillations and is sensitive to changes in the soil (Orlova et al. 2020).

Fig. 10. Evolution of R, Δt, N_Y, and the air temperature T during the experimental session with phase I–IV time regions. [Colour online]
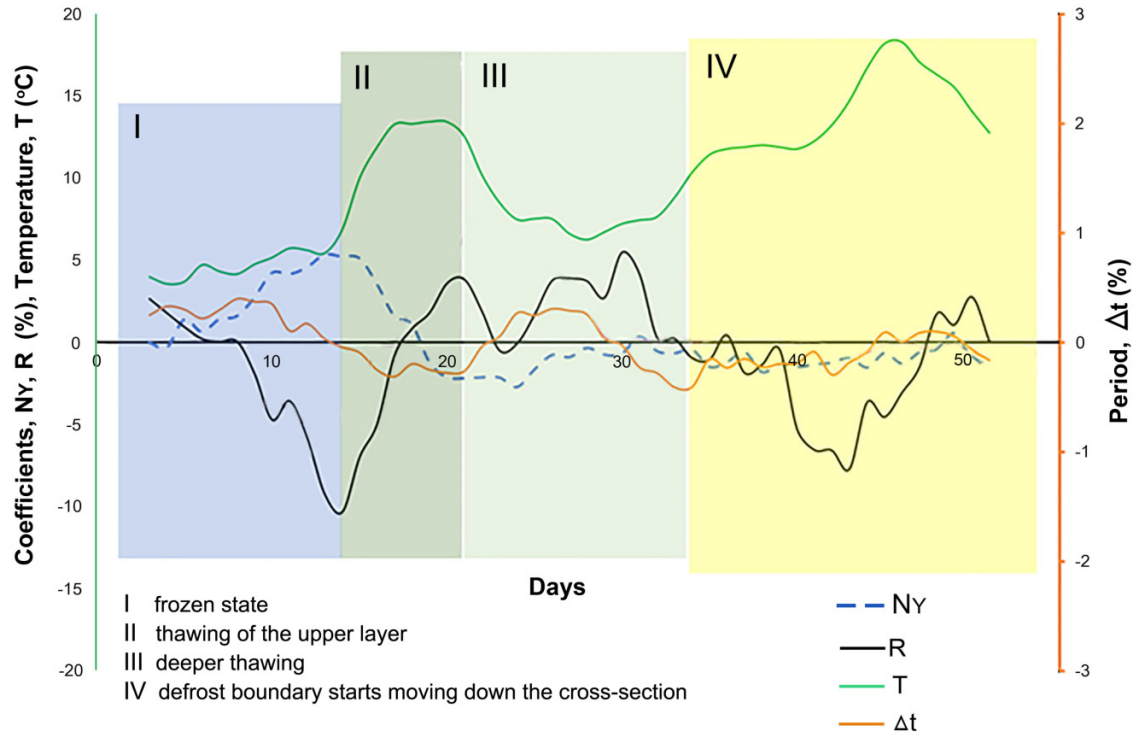
From days 10–30, the variation of R is similar to the variation of the temperature but with a phase delay of 2–3 days (*i*). Time interval Δt curve is in antiphase from the temperature curve during days 10–35 and then stabilizes (*ii*). Parameter N_Y shows positive fluctuations in the low-temperature part; however, when temperature rises, it goes down (*iii*) and stabilizes.

Let us compare these data to calculations based on the Elsasser model. It is reasonable to assume that high frequency characteristic N_Y is determined by the upper soil layer properties. Therefore, the positive fluctuations that occur before the temperature rise relate to relatively higher value of the shear modulus for frozen soil compared to the values during subsequent thawing (Terzaghi et al. 1996).

A possible explanation of the R minimum before the temperature spike is that the viscosity of the lower half-space is also the lowest. As T rises, a partial thawing takes place in the lower layer, which explains the phase shift of R relative to T. This agrees with data on partial thawing of ice in soils due to heating that occurs even at negative temperatures (Terzaghi et al. 1996). Seasonal soil freezing is estimated from existing regulatory standards for various regions of Russia. The viscosity in the interface area becomes lower; an increase of R is thus observed. The next minimum is hard to explain and we suggest it corresponds to a partial increase in the viscosity of the entire underlying layer due to processes with further heating.

The variation of time interval Δt behaves similar to R in 10–35-day period (*ii*). According to our model, its increase is either caused by the rise of viscosity or decline of the shear

modulus. The behavior of R_Y tells us that it is the latter. The further clarification of the observed patterns needs an elaborate study, and while there are no facts that suggest otherwise, we consider the proposed interactions as a satisfying physical description. To clarify the abovementioned development, we marked the corresponding phases on the time evolution chart in Fig. 10, which is a compact view of Fig. 9. Here, all fluctuations of R, Δt, N_Y are presented in percentiles of the total average value. Phase regions I–IV are as follows: I, frozen state; II, thawing of the upper layer; III, deeper thawing; IV, the defrost boundary starts moving down the cross-section.

While the suggested explanation is mostly qualitative, there are quantitative agreements as well. According to the Elsasser model, the seasonal variations of R and Δt identify approximately 10% of changes in shear modulus and viscosity. Such alterations of the deformation parameters correspond to 5% variations of the elastic wave velocity. This is an order of magnitude lower than the shifts that are attributed to be responsible for hazardous situations development, among which the thawing of frozen soils is paramount. The fundamental study of the relevant soils (Terzaghi et al. 1996) indicates that for frozen clay samples a change in their temperature by 1 °C leads to a change in the elasticity modulus by about 25%, and for frozen sands by up to 50%.

Conclusions

In the conditions of increasing traffic volumes and weight standards in railway transport, the task of improving

Can. Geotech. J. **00**: 1–12 (2022) | dx.doi.org/10.1139/cgj-2021-0621

9

methods of monitoring and diagnostics of subgrades on weak natural soils is of paramount importance for ensuring the railway communication safety. The monitoring technology advantages we are developing in comparison with episodic (discrete) surveys are (*i*) the possibility of detecting dangerous processes at an early stage, and (*ii*) specialized sources of external signals are not required and there is no violation of the train schedule.

The main limitations of the study at this stage are that we observed changes in the subgrade state in a relatively short time period and did not consider various types of seasonal changes such as freezing depth or soil temperature data of the project area. These questions are for future research.

Nevertheless, the fidelity of derived parameters on the first research step is well enough to detect possible dangerous developments in railway subgrade soils. We demonstrated this with an almost 2-month-long experimental session, and we did not employ any external signal sources but passing trains only. While no hazardous situation occurred within this period, the sensitivity was tested on the seasonal soil thawing. In our opinion, the simplicity of the setup and the automated nonstop monitoring and data processing may make this technique a valuable asset for the railroad safety assurance.

Acknowledgements

The authors thank our colleagues from OJSC Russian Railways for the opportunity to conduct research on the Severnaya Railway. Special thanks to Dr. Konstantin Moshkunov for constructive suggestions and discussions.

Article information

History dates

Received: 4 November 2021
Accepted: 30 June 2022
Accepted manuscript online: 4 July 2022
Version of record online: 4 November 2022

Copyright

© 2022 The Author(s). Permission for reuse (free in most cases) can be obtained from copyright.com.

Data availability

Seismic data are available upon official request from N. Laverov Federal Center for Integrated Arctic Research of the Ural Branch of the Russian Academy of Sciences (FECIAR UrB RAS), http://fciarctic.ru/ing.php?page=contact.

Author information

Author ORCIDs

Galina N. Antonovskaya https://orcid.org/ 0000-0002-8105-5892
Irina P. Orlova https://orcid.org/0000-0002-0014-7059

Author contributions

Galina Antonovskaya: data curation, funding acquisition, visualization, writing – original draft; Irina Orlova: data curation; Natalia Kapustian: data curation, methodology, writing – original draft, writing – review & editing.

Competing interests

The authors declare that they have no known competing financial interests or personal relationships that could have appeared to influence the work reported in this paper.

Funding Information

References

Anbazhagan, P., Lijun, S., Buddhima, I., and Cholachat, R. 2011. Model track studies on fouled ballast using ground penetrating radar and multichannel analysis of surface wave. Journal of Applied Geophysics, **74**(4): 175–184. doi:10.1016/j.jappgeo.2011.05.002.

Antonovskaya, G.N., Dobrovolsky, I.P., Kapustian, N.K., and Orlova, I.P. 2021. Determination of the in situ elastic properties of a railway roadbed by seismic observations. Seismic Instruments, **57**(1): 1–8. doi:10.3103/S0747923921010023.

Antonovskaya, G.N., Kapustian, N.K., and Basakina, I.M. 2020a. New approach of railway roadbed state monitoring using broadband seismometers. *In* Transportation Soil Engineering in Cold Regions. *Edited by* A. Petriaev and A. Konon Lecture Notes in Civil Engineering **49**. doi:10.1007/978-981-15-0450-1_13.

Antonovskaya, G.N., Kapustian, N.K., and Fedorenko, E.V. 2020b. Capabilities of seismic equipment in assessing the state of railway embankments. Seismic Instruments, **56**(2): 161–169. doi:10.3103/S0747923920020024.

Ashpiz, E.S., Khrustalev, L.N., and Vavrinuk, T.S. 2011. Accounting for breach of natural heat exchange in the design of railway in permafrost soil. Physics Procedia, **22**: 130–135. doi:10.1016/j.phpro.2011.11.021.

Authority Transport Asset Standards. 2021. Geotechnical Instrumentation and Monitoring Guidelines. T MU CI 12140 GU. Version 2.0.

Aw, E.S. 2007. Low cost monitoring system to diagnose problematic rail bed: case study at a mud pumping site. Thesis (PhD) Massachusetts Institute of Technology, Dept. of Civil and Environmental Engineering. https://dspace.mit.edu/handle/1721.1/42051.

Bachrach, R., and Nur, A. 1998. High-resolution shallow-seismic experiments in sand, part I: Water table, fluid flow, and saturation. Geophysics, **63**(4): 1225–1233. doi:10.1190/1.1444423.

Basakina, I., Antonovskaya, G., Kapustian, N., and Pudova, I. 2014. New seismic methods for the historical constructions diagnostics. *In* Second European Conference on Earthquake Engineering and Seismology. Instambul. 25–29 August 2014. http://www.eaae.org/Media/Default/2ECCES/2ecces_eaae/454.pdf.

Brough, M., Stirling, A., Ghataora, G., and Madelin, K. 2003. Evaluation of railway trackbed and formation: a case study. NDT & E International, **36**(3): 145–156. doi:10.1016/S0963-8695(02)00053-1.

Brzeziński, K., Rybicki, T., and Józefiak, K. 2018. Analysis of stability of railway embankment including horizontal forces in light of Eurocode. MATEC Web of Conferences, **196**: 03016. doi:10.1051/matecconf/201819603016.

Burdzik, R., and Nowak, B. 2017. Identification of the vibration environment of railway infrastructure. Procedia Engineering, **187**: 556–561. doi:10.1016/j.proeng.2017.04.414.

Carslaw, H.S., and Jaeger, J.C. 1989. Conduction of heat in solids. 2nd ed. Journal of Engineering Materials and Technology, **108**: 378–378. doi:10.1115/1.3225900.

Connolly, D.P., Kouroussis, G., Giannopoulos, A., Verlinden, O., Woodward, P.K., and Forde, M.C. 2014a. Assessment of railway vibrations

ment failure experiment. A general summary. Research Reports of
the Finnish Transport Agency, **29**: 57.

Lopes, P., Ruiz, J.F., and Alves Costa, P. 2016. Vibrations inside build-
ings due to subway railway traffic. Experimental validation of a
comprehensive prediction model. Science of the Total Environ-
ment, **568**: 1333–1343. doi:10.1016/j.scitotenv.2015.11.016. PMID:
26589136.

Ma, W., Wen, Z., Sheng, Yu, Wu, Q., Wang, D., and Feng, W. 2012. Remedy-
ing embankment thaw settlement in a warm permafrost region with
thermosyphons and crushed rock revetment. Canadian Geotechnical
Journal, **49**(9): 1005–1014. doi:10.1139/t2012-058.

Mashinskii, E.I. 2005. Experimental study of the amplitude effect on
wave velocity and attenuation in consolidated rocks under confin-
ing pressure. Journal of Geophysics and Engineering, **2**(3): 199–212.
doi:10.1088/1742-2132/2/3/004.

McHenry, M.T., and Rose, J.G. 2012. Railroad subgrade support and per-
formance indicators: a review of available laboratory and in-situ test-
ing methods. Kentucky Transportation Center Research Report, **12**.
http://dx.doi.org/10.13023/KTC.RR.2012.02.

Mirzaxidova, O.M. 2020. Diagnostics of the roadbed. International Jour-
nals of Sciences and High Technologies. **Special Issue August**: 41–43.
doi:10.52155/ijpsat.v0.0.2053.

Mukhamediev, S.A., Grachev, A.F., and Yunga, S.L. 2008. Nonstationary
dynamic control of seismic activity of platform regions by mid-ocean
ridges. Izvestiya. Physics of the Solid Earth, **44**: 9–17.

NetworkRail. 2018. Earthworks Technical Strategy. Available from
https://www.networkrail.co.uk/wp-content/uploads/2018/07/Earthwo
rks-Technical-Strategy.pdf.

Ngamkhanong, C., Kaewunruen, S., and Costa, B.J.A. 2018. State-of-the-
art review of railway track resilience monitoring. Infrastructures, **3**:
3. doi:10.3390/infrastructures3010003.

Orlova, I.P., Kapustian, N.K., Antonovskaya, G.N., and Basakina, I.M. 2020.
Possibilities of seismic equipment for roadbed railway monitoring in
areas with difficult ground conditions. Vestnik of Geosciences, **4**(304):
33–39. doi:10.19110/geov.2020.4.5.

Picoux, B., and LeHouédec, D. 2005. Diagnosis and prediction of vibration
from railway trains. Soil Dynamics and Earthquake Engineering, **25**:
905–921. doi:10.1016/j.soildyn.2005.07.002.

Pinzon-Rincon, L., Lavoué, F., Mordret, A., Boué, P., Brenguier, F. Dales,
P., et al. 2021. Humming trains in seismology: an opportune source
for probing the shallow crust. Seismological Research Letters, **92**(2A):
623–635. doi:10.1785/0220200248.

Railvolution. 2019. Russia: Advantages of Using Wagons with
Greater Payload Capacity. [Online]. Available from http:
//www.railvolution.net/news/russia-advantages-of-using-wagons-
with-greater-payload-capacity.

Russian Railways company standard 10.002–2015. 2016. Innovative
freight cars. Rules for evaluating economic efficiency.

Shalev, E., Kurzon, I., Doan, M.-L., and Lyakhovsky, V. 2015. Water-level
oscillations caused by volumetric and deviatoric dynamic strains.
Geophysical Journal International, **204**: 841–851.

Stoyanovich, G.M., and Pupatenko, V.V. 2015. Propagation of vibrations
in thawing deep seasonally frozen soils in railway subgrade. Sci-
ences in Cold and Arid Regions, **7**(5): 0534–0540. doi:10.3724/SP.J.
1226.2015.00534.

Sukhobok, Y.A., Pupatenko, V.V., Stoyanovich, G.M., and Ponomarchuk,
Y.V. 2016. Soil formation lithological profiling using ground pene-
trating radar. Procedia Engineering, **143**: 1236–1243. doi:10.1016/j.
proeng.2016.06.110.

Szwilski, T.B., Begley, R., Ball, J., and Dailey, P. 2003. Application of geo-
physical methods to evaluate rail-track subsurface. Symposium on
the Application of Geophysics to Engineering and Environmental
Problems Proceedings: 794–802. doi:10.4133/1.2923225.

Szwilski, T., Begley, R., Dailey, P., and Sheng, Z. 2004. Using geophysi-
cal techniques to study rail track in an area of ground movement.
Geotechnical Engineering for Transportation Projects. GSP 126. doi:
10.1061/40744(154)149.

Terzaghi, K., Peck, R.B., and Mesri, G.(Eds.) 1996. Soil Mechanics in Engi-
neering Practice. 3rd ed. ISBN: 978-0-471-08658 -1.

Tian, Y., Yang, Z., Liu, Y., Cai, X., and Shen, Y. 2021. Long-term thermal
stability and settlement of heat pipe-protected highway embankment
in warm permafrost regions. Engineering Geology, **292**. doi:10.1016/
j.enggeo.2021.106269.

Trnkoczy, A. 2012. Understanding and parameter setting of STA/LTA trig-
ger algorithm. *In* New Manual of Seismological Observatory Practice 2

using an efficient scoping model. Soil Dynamics and Earthquake En-
gineering, **58**: 37–47. doi:10.1016/j.soildyn.2013.12.003.

Connolly, D.P., Kouroussis, G., Woodward, P.K., Alves Costa, P., Verlinden,
O., and Forde, M.C. 2014b. Field testing and analysis of high speed rail
vibrations. Soil Dynamics and Earthquake Engineering, **67**: 102–118.
doi:10.1016/j.soildyn.2014.08.013.

Crane, J.M. 2013. Effects of stress and water saturation on seismic veloc-
ity and attenuation in near surface sediments. LSU Doctoral Disser-
tations. **3714**. https://digitalcommons.lsu.edu/gradschool_dissertatio
ns/3714.

Donohue, S., Gavin, K., and Tolooiyan, A. 2011. Geophysical and geotech-
nical assessment of a railway embankment failure. Near Surface Geo-
physics, **9**(1): 33–44. doi:10.3997/1873-0604.2010040.

Elsasser, W.M. 1971. Two-layer model of upper-mantle circulation. Jour-
nal of Geophysical Research, **76**(20): 4744–4753.

Fontul, S., Paixão, A., Solla, M., and Pajewski, L. 2018. Railway track con-
dition assessment at network level by frequency domain analysis of
GPR data. Remote Sensing, **10**: 559. doi:10.3390/rs10040559.

Fraga-Lamas, P., Fernández-Caramés, T.M., and Castedo, L. 2017. Towards
the internet of smart trains: a review on industrial IoT-Connected
railways. Sensors, **17**(6): 1457. doi:10.3390/s17061457.

Garagulia, L.S., Ershov, E.D. 2000. Geocryological Hazards, Nat. Hazards
Russ. Ser. *Edited by* V.I. Osipov and S.K. Shoigu. Moscow. 315pp.

Grassie, S.L., Gregory, R.W., Harrison, D., and Johnson, K.L. 1982. The dy-
namic response of railway track to high frequency vertical excitation.
ARCHIVE: Journal of Mechanical Engineering Science 1959–1982
(vols 1–23), **24**: 97–102. doi:10.1243/JMES_JOUR_1982_024_018_02.

Gupta, H.K., and Rustogi, B.K. 1976. Dams and Earthquakes. Elsevier, Am-
sterdam.

Hendry, M., Martin, D., Barbour, S., and Edwards, T. 2008. Monitoring
cyclic strain below a railway embankment overlying a peaty foun-
dation using novel instrumentation. *In* 61st Canadian Geotechnical
Conference, Edmonton, Alberta, 21–24 September. No. 443.

Hu, J., Luo, Y., Ke, Z., Liu, P., and Xu, J. 2018. Experimental study on
ground vibration attenuation induced by heavy freight wagons on
a railway viaduct. Journal of Low Frequency Noise, Vibration and Ac-
tive Control, **37**(4): 881–895. doi:10.1177/1461348418765949.

Irvine, T. 2013. Shock and vibration stress as a function of velocity. Revi-
sion G. http://www.vibrationdata.com/tutorials_alt/sv_velocity.pdf.

Ižvolt, L., Dobeš, P., and Pultznerová, A. 2016. Monitoring of moisture
changes in the construction layers of the railway substructure body
and its subgrade. Procedia Engineering, **161**: 1049–1056. doi:10.1016/
j.proeng.2016.08.847.

Kapustian, N.K., and Yudakhin, F.N. 2007. Seismic studies of technogenic
impacts on the Earth's crust and their consequences. Yekaterinburg:
Ural Branch of the Russian Academy of Sciences, 416 (in Russian).

Kondratiev, V.G. 2017. Main geotechnical problems of railways and roads
in Kriolitozone and their solutions. Procedia Engineering, **189**: 702–
709. doi:10.1016/j.proeng.2017.05.111.

Kotlyakov, V., and Khromova, T. 2012. Permafrost. Land Resources of
Russia. International Institute for Applied Systems Analysis. http:
//webarchive.iiasa.ac.at/Research/FOR/russia_cd/perm_des.htm.

Kovacevic, M.S., Gavin, K., Stipanovic Oslakovic, I., and Bacic, M. 2016.
A new methodology for assessment of railway infrastructure condi-
tion. Transportation Research Procedia, **14**: 1930–1939. doi:10.1016/
j.trpro.2016.05.160.

Kovalevsky, V.V., Glinsky, B.M., Khairetdinov, M.S., Fatyanov, A.G., Kar-
avaev, D.A. Braginskaya, L.P., et al. 2020. Chapter 1.3—active vi-
bromonitoring: experimental systems and fieldwork results. Active
Geophysical Monitoring. 2nd ed. *Edited by* J. Kasahara, M.S. Zh-
danov and H. Mikada. pp. 43–65. ISBN 9780081026847. doi:10.1016/
B978-0-08-102684-7.00003-0.

Krylov, V.V. 1997. Spectra of low frequency ground vibrations gener-
ated by high speed trains on layered ground. Journal of Low Fre-
quency Noise, Vibration & Active Control, **16**(4): 257–270. doi:10.
1177/026309239701600404.

Kudryavtsev, S., Kazharsky, A., Valtseva, T., Kotenko, Z., and Goncharova,
E. 2016. Thermophysical feasibility of railway embankment design on
permafrost when projecting side tracks. Procedia Engineering, **165**:
1080–1086. doi:10.1016/j.proeng.2016.11.822.

Lehtonen, V. 2011. Instrumentation and analysis of a railway embank-

(NMSOP-2). *Edited by* P. Bormann. Deutsches Geo Forschungs Zentrum GFZ, Potsdam. pp. 1–20. doi:0.2312/GFZ.NMSOP-2_IS_8.1.

Varlamov, S. 2018. Thermal monitoring of railway subgrade in a region of ice-rich permafrost, Yakutia, Russia. Cold Regions Science and Technology, **155**: 184–192. doi:10.1016/j.coldregions.2018.06.016.

Weber, M., and Münch, U.(Eds). 2014. Tomography of the Earth's Crust: From Geophysical Sounding to Real-Time Monitoring. GEOTECHNOLOGIEN Science Report No. 21. doi:10.1007/978-3-319-04205-3.

Zaima, K., and Katayama, I. 2018. Evolution of elastic wave velocities and amplitudes during triaxial deformation of Aji granite under dry and water-saturated conditions. Journal of Geophysical Research: Solid Earth, **123**: 9601–9614. doi:10.1029/2018JB016377.

Zhang, A.A., Ashpiz, E.S., Khrustalev, L.N., and Shesternev, D.M. 2018. A new way for thermal stabilization of permafrost under railway embankment. Kriosfera Zemli, **XXII**(3): 59–62. doi:10.21782/EC2541-9994-2018-3(59-62).